Direct observation of backbone planarization via side-chain alignment in single bulky-substituted polythiophenes

Dominic Raithel[a], Lena Simine[b], Sebastian Pickel[a], Konstantin Schötz[c], Fabian Panzer[c], Sebastian Baderschneider[a], Daniel Schiefer[d], Ruth Lohwasser[e], Jürgen Köhler[a,f], Mukundan Thelakkat[e], Michael Sommer[d,1], Anna Köhler[c,f], Peter J. Rossky[b], and Richard Hildner[a,2]

[a]Experimental Physics IV, University of Bayreuth, 95440 Bayreuth, Germany; [b]Department of Chemistry, Rice University, Houston, TX 77005; [c]Experimental Physics II, University of Bayreuth, 95440 Bayreuth, Germany; [d]Institute of Macromolecular Chemistry, University of Freiburg, 79104 Freiburg, Germany; [e]Applied Functional Polymers, University of Bayreuth, 95440 Bayreuth, Germany; and [f]Bayreuth Institute of Macromolecular Research, University of Bayreuth, 95440 Bayreuth, Germany

Edited by Michael L. Klein, Temple University, Philadelphia, PA, and approved February 2, 2018 (received for review November 5, 2017)

The backbone conformation of conjugated polymers affects, to a large extent, their optical and electronic properties. The usually flexible substituents provide solubility and influence the packing behavior of conjugated polymers in films or in bad solvents. However, the role of the side chains in determining and potentially controlling the backbone conformation, and thus the optical and electronic properties on the single polymer level, is currently under debate. Here, we investigate directly the impact of the side chains by studying the bulky-substituted poly(3-(2,5-dioctylphenyl)thiophene) (PDOPT) and the common poly(3-hexylthiophene) (P3HT), both with a defined molecular weight and high regioregularity, using low-temperature single-chain photoluminescence (PL) spectroscopy and quantum-classical simulations. Surprisingly, the optical transition energy of PDOPT is significantly (∼2,000 cm^{-1} or 0.25 eV) red-shifted relative to P3HT despite a higher static and dynamic disorder in the former. We ascribe this red shift to a side-chain induced backbone planarization in PDOPT, supported by temperature-dependent ensemble PL spectroscopy. Our atomistic simulations reveal that the bulkier 2,5-dioctylphenyl side chains of PDOPT adopt a clear secondary helical structural motif and thus protect conjugation, i.e., enforce backbone planarity, whereas, for P3HT, this is not the case. These different degrees of planarity in both thiophenes do not result in different conjugation lengths, which we found to be similar. It is rather the stronger electronic coupling between the repeating units in the more planar PDOPT which gives rise to the observed spectral red shift as well as to a reduced calculated electron–hole polarization.

conjugated polymers | single-molecule spectroscopy | quantum-classical atomistic simulations | side-chain engineering | organic electronics

Device applications of conjugated polymers are strongly determined by their structural, electronic, and optical properties. However, the design of new polymers is not straightforward, as often conflicting demands have to be satisfied simultaneously to achieve optimum device performance (1). For instance, application in organic light-emitting diodes requires strong and efficient emission as well as efficient transport of injected charges. The charge transport characteristics strongly depend on film morphology, orientation with respect to interfaces, and the strength of interchain interactions (2). However, dense packing of conjugated polymers into typically π–π-type arrangements reduces emission quantum yield. Hence, suppression of π stacking, while maintaining high intrachain and interchain order, is important for lighting applications (3).

To manipulate and optimize the relevant structural and electronic properties of conjugated polymers for specific applications, side-chain engineering has emerged as a versatile toolkit in recent years (note that "side-chain engineering" is to be understood here in its widest sense, i.e., direct backbone substitution with heteroatoms and modifying large side groups) (4–8). Noncovalent interactions between backbone and substituents (e.g., CH···S, CH···F, CH···O, or F···S interactions) have a strong impact on the backbone conformation of isolated chains (9). In combination with interactions between chains, such as π–π- or hydrogen-bonding interactions, which direct self-assembly, the resulting film morphologies can be controlled (10). In particular, fluorination has attracted attention, because it can introduce steric interactions with neighboring groups and thus modify backbone conformation (10). Moreover, fluorine possesses the highest electronegativity, which was shown to stabilize the highest occupied molecular orbital (HOMO) and/or lowest unoccupied molecular orbital (LUMO; see e.g., ref. 5 for a recent review). However, disentangling structural and electronic effects of fluorination is very challenging (4). An alternative approach is to increase the density or bulkiness of side groups. For example, enhancing the side-chain density of a donor–acceptor copolymer, which is widely used for organic solar cells, improved its luminescence properties significantly, thus allowing for application in light-emitting devices (11). Appending sterically demanding groups like dendrimers (12) stiffens the backbone through steric repulsion

Significance

Conjugated polymers are promising materials for flexible electronics and photovoltaics. Recent progress in polymer design led to a rise in device efficiency. Tailoring intramolecular interactions is a central design element, which allows fine-tuning of optical and electronic properties. However, prediction and measurement of intrinsic properties of newly synthesized polymers is challenging, as they are often hidden by ensemble effects. Single-molecule spectroscopy allows revelation of the intrinsic changes upon chemical modification, here specifically a variation of the side chains. Surprisingly, a more disordered, bulky side chain leads to a higher order and better conjugation within the electronically active backbone of a single chain. This study gives detailed insights into changes in photophysical properties and suggests new ideas for synthesis.

Author contributions: L.S., P.J.R., and R.H. designed research; D.R., L.S., S.P., K.S., and F.P. performed research; S.B., D.S., R.L., M.T., and M.S. contributed new reagents/analytic tools; D.R., L.S., S.P., K.S., and R.H. analyzed data; D.R., L.S., S.P., K.S., J.K., A.K., P.J.R., and R.H. interpreted data; and D.R., L.S., and R.H. wrote the paper.

The authors declare no conflict of interest.

This article is a PNAS Direct Submission.

[1]Present address: Polymerchemie, Technische Universität Chemnitz, 09111 Chemnitz, Germany.

[2]To whom correspondence should be addressed. Email: richard.hildner@uni-bayreuth.de.

This article contains supporting information online at www.pnas.org/lookup/suppl/doi:10.1073/pnas.1719303115/-/DCSupplemental.

of neighboring side chains. The resulting increase in persistence length was recently highlighted as a new design aspect to optimize optical absorption and thus solar cell performance (13). However, a high persistence length alone is not sufficient; only a concomitant backbone planarization enhances absorption due to an increase in transition dipole moment (14–16). However, more bulky side groups are usually associated with a larger torsion of the conjugated backbone, i.e., with a large distribution of interring dihedral angles (17–19), which localizes electronic excitations and gives rise to less favorable material properties.

Here, we show that, contrary to this common notion, bulky side chains can force the backbone of conjugated polymers into a more planar conformation via side-chain alignment. We combine single-molecule low-temperature photoluminescence (PL) spectroscopy with quantum-classical atomistic simulations to investigate two polythiophenes with defined molecular weight and high regioregularity but different substitution patterns (Fig. 1 *D–F*, *Insets*): First, poly(3-(2,5-dioctylphenyl)thiophene) (PDOPT) with sterically very demanding 2,5-dioctylphenylene side-chains, which prevent direct π–π interaction of neighboring backbones (20, 21). Second, the prototypical poly(3-hexylthiophene) (P3HT) with relatively short hexyl side groups. For P3HT, interchain π–π interactions play an important role and determine the transition energy, to a large extent (22). Particularly, this latter system was studied extensively by ensemble (16, 23–25) and single-molecule spectroscopy (26–28).

We find that the PDOPT single-chain PL spectra are strongly red-shifted by >2,000 cm^{-1} (>0.25 eV) with respect to P3HT, which is not obvious from the corresponding, very similar ensemble spectra (Fig. S1). We were able to ascribe this substantial spectral shift to side-chain induced backbone planarization in PDOPT that increases the electronic coupling between repeating units. This is accompanied by a reduction in the difference between the centers of mass of the electron/hole wave functions—the electron–hole polarization (29), which is a measure for the charge transfer character of the excited state.

Results and Discussion

PL Spectroscopy of Single PDOPT Chains. We investigated two PDOPT samples, PDOPT16 and PDOPT89, with number average molecular weights of M_n = 6.1 kDa (~16 repeating units, PDOPT16 with a dispersity of 1.07 and a regioregularity of >93%), and M_n = 33.7 kDa (~89 repeating units, PDOPT89 with a dispersity of 1.66 and a regioregularity of >98%); see *Methods and Materials* and *SI Methods and Materials*. Fig. 1 *A* and *B* depicts two representative single-chain PL spectra of PDOPT16 and PDOPT89 after partial temporal averaging (see *SI Methods and Materials*). Both spectra show a prominent zero-phonon line (ZPL) at 17,022 cm^{-1} and 16,777 cm^{-1} with line widths of 33 cm^{-1} and 64 cm^{-1} (FWHM) for PDOPT16 and PDOPT89, respectively. A broad phonon-side band appears in the low-energy shoulder of the ZPLs and indicates weak electron–phonon coupling to low-energy vibrational modes of the backbone or the host matrix (30, 31). The dominating vibrational transition is offset from the ZPL by around 1,480 cm^{-1} to lower energies and is associated with aromatic carbon-bond stretching modes (32). The PL spectra of PDOPT16 feature only one ZPL (Fig. 1*A*), i.e., only a single emitting site per chain as expected from the effective conjugation length of approximately eight repeating units for polythiophenes (33–36). In contrast, for PDOPT89, we observe two additional weak lines at high energies (Fig. 1*B*, asterisks). The independent blinking and spectral diffusion of these weak peaks (Fig. S2) demonstrates multichromophoric behavior with several emitting sites (ZPLs) per chain.

We evaluated, in total, 88 (102) ZPLs of PDOPT16 (PDOPT89) by fitting Gaussian or Lorentzian functions to their high-energy tails. The resulting histograms of the ZPL width (Fig. 1 *D* and *E*) and ZPL energy (Fig. 1 *G* and *H*) show only a little difference between the systems. The average ZPL width (FWHM) is 70 cm^{-1} for the short and 67 cm^{-1} for the long chains. Both distributions are very broad, with maximum ZPL widths of ~250 cm^{-1}. For other conjugated polymers, such as P3HT (22) and ladder-type poly(*p*-phenylenes) (37), we showed that the ZPLs are broadened by unresolved spectral diffusion, i.e., by random jumps of the transition energy on time scales faster than the temporal resolution of our measurement (here

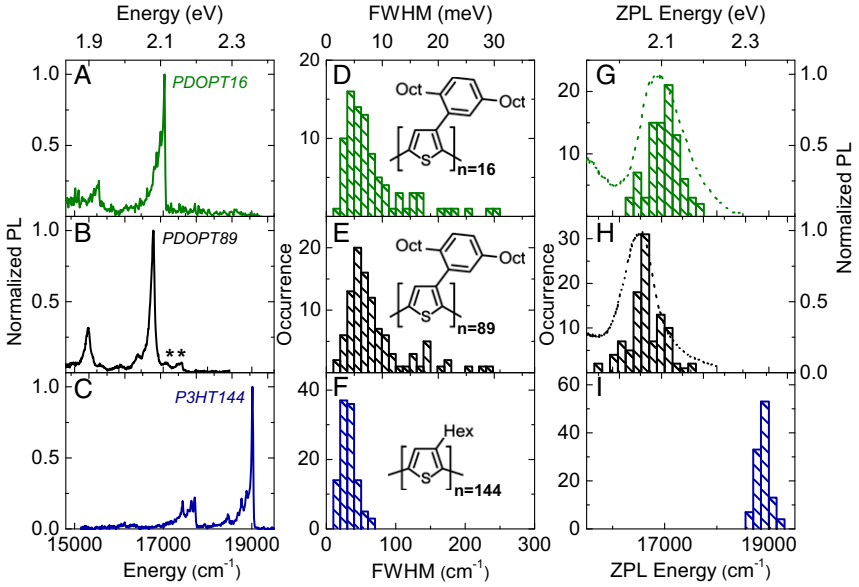

Fig. 1. Low-temperature PL spectroscopy on single polythiophene chains. (*A* and *B*) Single-chain PL spectra of poly(3-(2,5-dioctylphenyl)-thiophene), PDOPT, for two different chain lengths embedded in *n*-hexadecane. (*C*) Single-chain PL spectrum of poly(3-hexyl-thiophene), P3HT, in *n*-hexadecane. (*D–F*) Distributions of line widths (FWHM) of the ZPL. (*G–I*) Distributions of spectral positions of the ZPLs. The dashed lines in *G* and *H* are low-temperature ensemble PL spectra of the corresponding matrix-isolated PDOPT sample (in *n*-hexadecane). In *D–F*, the chemical structures are shown as *Insets*; n denotes the mean number of repeating units, and Oct and Hex stand for *n*-octyl and *n*-hexyl groups. The peaks in *B* marked with asterisks denote additional weak ZPLs from the same single PDOPT chain (see also Fig. S2). The data in *C*, *F*, and *I* are taken from ref. 22.

1 s to 3 s). This dynamic disorder is induced by structural fluctuations of groups of atoms or molecules in the local environment of the emitting site (31, 37–40). Accordingly, we ascribe the broad ZPLs of PDOPT to unresolved spectral diffusion processes as well.

For PDOPT16 (PDOPT89), the histograms of ZPL energies range from 16,276 cm^{-1} to 17,738 cm^{-1} (15,787 cm^{-1} to 17,480 cm^{-1}) and are centered around 16,975 cm^{-1} (16,633 cm^{-1}); see Fig. 1 *G* and *H*. The electronic transition of the corresponding low-temperature matrix-isolated ensemble spectra (dashed lines, Fig. 1 *G* and *H*) with maxima at 16,858 cm^{-1} (PDOPT16) and 16,505 cm^{-1} (PDOPT89) provide good envelopes to these histograms. We attribute the red shift of about 350 cm^{-1} from PDOPT16 to PDOPT89 in both single-chain and bulk data to intrachain downhill energy transfer within the multichromophoric PDOPT89 chains. Such energy transfer rapidly populates predominantly lower-energy emitting sites (41), whereas higher-energy sites are only weakly emitting (Fig. 1*B*, asterisks) or do not emit at all. In contrast, for PDOPT16 with only a single emitting site, the ZPL distribution is entirely determined by dispersive interactions of the emitting site with the local environment (42, 43) as well as by the degree of planarity of the polymer backbone, both of which vary for each chain (43–45).

PDOPT vs. P3HT. It is now interesting to compare our PDOPT single-chain data with those of the prototypical P3HT that we have reported recently (Fig. 1 *C*, *F*, and *I* and ref. 22). The P3HT samples investigated possess an M_n of 2.6 kDa (~16 repeating units, P3HT16 with a dispersity of 1.17 and a regioregularity >93%) and an M_n of 24 kDa (~144 repeating units, P3HT144 with a dispersity of 1.15 and a regioregularity >98%). For both PDOPT and P3HT, there is no difference between the corresponding spectra of short and long chains (Fig. 1 and Fig. S3), and we thus focus on the long chains (PDOPT89 and P3HT144) in the following discussion.

Dynamic and static disorder. The first obvious differences are the on average significantly broader ZPLs of PDOPT with respect to those of P3HT (mean ZPL width 67 cm^{-1} and 32 cm^{-1}, respectively, Fig. 1 *E* and *F*). These data indicate a high degree of dynamic disorder in PDOPT due to very pronounced spectral diffusion processes with large unresolved spectral jumps compared with P3HT. The magnitude of these jumps increases with decreasing distance between the thiophene backbone and the fluctuating unit in its local environment (31, 42, 46). We therefore suggest that this strong spectral diffusion in PDOPT originates from librational motions of its side-group phenyl rings (47, 48), which are directly appended to the conjugated backbone.

Furthermore, for PDOPT, the inhomogeneous width (FWHM) of the distribution of ZPL energies is larger by a factor of 2.5 (PDOPT89, 770 cm^{-1}; P3HT144, 300 cm^{-1}; see Fig. 1 *H* and *I*), indicating a higher static disorder in comparison with P3HT. The only difference between the samples is the more bulky side group of PDOPT, and thus steric effects induced by these groups probably play an important role (*vide infra*). These observations demonstrate that the side groups possess a strong influence on the photophysics of polythiophenes that is not obvious from ensemble PL data alone (Fig. S1).

ZPL energies. The most unexpected finding is that the ZPL energies of single PDOPT chains are red-shifted by more than 2,200 cm^{-1} (0.27 eV) in comparison with P3HT (Fig. 1 *H* and *I*). We have recently shown, by calculations on thiophene derivatives, that the transition energy of the absorbing/emitting sites red-shift by up to 4,800 cm^{-1} (0.6 eV) for increasing planarity (22, 29), in agreement with other reports (36, 44, 45, 49). Based on this work, we propose that the observed red shift between isolated PDOPT and P3HT is largely caused by backbone planarization in PDOPT, at least on length scales of an emitting site, via noncovalent interactions with the bulky side groups (7, 9). A further factor, that may in part contribute to this red shift, is the more polarizable local environment for the emitting sites (50, 51) provided by the aromatic phenyl rings of PDOPT compared with the hexyl groups of P3HT.

Ensemble PL spectroscopy: Planarization preceding aggregation. Independent evidence for our hypothesis comes from temperature-dependent PL spectroscopy on solutions of PDOPT89 and P3HT144. This approach yields insights into the aggregation process upon cooling (16); in particular, we found that an initial backbone planarization of the disordered solution phase occurs before the transition to the aggregated phase. The signature of this initial planarization is a continuous red shift of the solution PL spectrum with decreasing temperature.

For both PDOPT and P3HT dissolved in THF, we quantified the spectral red shifts of the disordered phase by fitting the temperature-dependent PL spectra (Fig. 2, *Inset*) with Franck–Condon (FC) progressions (16) and retrieving the energies of the purely electronic (0–0) transition (Fig. 2 and *SI Franck–Condon Analysis*). A linear fit to the temperature-dependent 0–0 positions reveals an average red shift of 1.6 cm^{-1}/K for PDOPT (black) and 4.1 cm^{-1}/K for P3HT (blue). Note that the transition from disordered chains to aggregates occurs at 180 K for PDOPT and at 240 K for P3HT. Hence, the initial rate of red shift upon cooling (but before aggregation) is less pronounced for PDOPT than for P3HT, as can be expected for a more planar chain and from our single-chain data. Similar experiments on methyl-substituted ladder-type poly(*para*-phenylene) (MeLPPP) (52) result in a very small slope of about 0.60 cm^{-1}/K. Since the rigid rod-like MeLPPP represents the prototype of a highly planar system, these ensemble data provide further evidence that PDOPT possesses a rather planar conformation in solution—a conformation in which we expect PDOPT chains to exist in our single-molecule experiments as well owing to the rapid cooling procedure during sample preparation (22).

Quantum-Classical Atomistic Simulations. To gain further insight into the origin of the pronounced red shift of the ZPLs between PDOPT and P3HT, we performed quantum-classical atomistic simulations of PDOPT16 and compared with our recent results for P3HT (29). Following the same protocol as in ref. 29, we used a modified Quantum Mechanical Consistent Force Field for π-electrons (QCFF/PI) method (53, 54) to generate a thermal ensemble of single PDOPT16 at room temperature (298 K), by generating 1,000 structures and running a thermal trajectory for ~1 ns. We then calculated the optical and electronic properties using the semiempirical Pariser–Parr–Pople (PPP) Hamiltonian for π-electrons at the level of configuration interaction singles

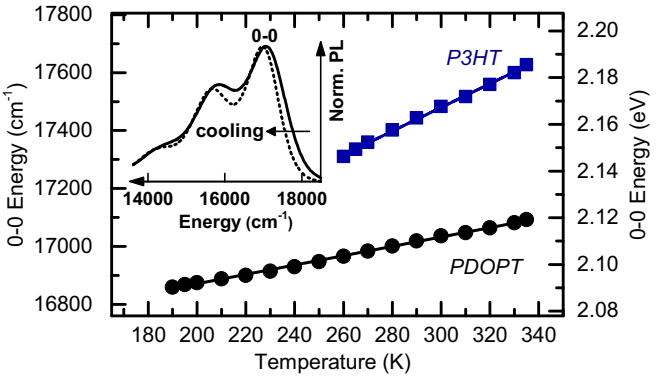

Fig. 2. Temperature-dependent solution PL spectra. Shown is evolution of the 0–0 peak position of the ensemble PL spectra of the disordered solution phase of PDOPT89 (black circles) and P3HT144 (blue squares) dissolved in THF. The solid lines are linear fits to the data points. (*Inset*) The solution PL spectra of PDOPT89 at a temperature of 300 K (solid line) and 240 K (dashed line).

(CIS). The choice of high temperature was motivated by the experimental conditions, in which the rapid cooling of the sample is expected to trap the molecules in typical high-temperature conformations. For details of the simulations, see *Methods and Materials* and *SI Simulation Protocol*.

Backbone and side-chain conformations. For PDOPT, we initialized our molecular dynamics simulations with single PDOPT16 structures similar to those in crystals (20) with all thiophene units in trans configuration (interring dihedral angle $\phi = 180°$), and with the phenyl rings at 90° to the backbone. The torsional free energy, calculated as potential of mean force [PMF $= -k_BT \log P(\phi)$], shows a minimum at 180° (Fig. 3*A*), which reflects a stable transplanar backbone. The minimum is rather flat, and thus a large set of dihedral angles is thermally accessible, which allows for a large degree of torsional disorder—the variation around the mean angle—in agreement with our single-chain data. The *n*-octyl chains on adjacent monomers were found to form stable contacts, which lead to the emergence of helical wrapping, resembling barber's pole stripes, around the thiophene backbone (Fig. 3*B*). These contacts stabilize the perpendicular orientation between thiophene and phenyl units, and balance steric repulsions leading to the backbone planarization.

In contrast, in single-molecule P3HT, the backbone is more exposed, and side chains do not form an identifiable structural motif. We recently showed that the PMF of P3HT (see Fig. 3*A*) possesses a clear minimum around a dihedral angle of $\phi = 145°$ (29), and, in consequence, the chain conformation is rather disordered, as illustrated in Fig. 3*A*, *Top*. This behavior is in line with other work on P3HT, in which repulsive S···H interactions between the sulfur atom and the hydrogen atoms of the closest methylene unit in the adjacent hexyl group were shown to lead to nonplanar optimal structures (27, 32, 49, 55).

Optical and electronic properties. Our simulated absorption spectra of the thermal ensembles of PDOPT and P3HT at room temperature are depicted in Fig. 3*C*. Notably, they exhibit a spectral shift of *ca.* 2,000 cm^{-1}, in good quantitative agreement with our experiments. These results clearly show that the observed differences in backbone conformation between PDOPT and P3HT, induced by very different side groups, result in the experimentally measured, profoundly distinct optical properties.

We further calculated a coherence length L and an electron–hole displacement distance $R_{e\text{-}h}$. L is a measure for the size of the emitting/absorbing sites ("chromophores") and is defined as the "radius of gyration" of the exciton wave function (56). $R_{e\text{-}h}$ is computed as the difference between the centers of mass of the electron/hole wave functions, and is a measure of electron–hole polarization, i.e., of the charge transfer character of the excited state. Interestingly, the calculated coherence lengths L are similar for both systems, ~6.5 repeating units; see Fig. 3*D*. This finding is rather surprising, as the spectral red shift would conventionally be interpreted as being due to an increase in L, or chromophore size, because of the planarization of the PDOPT backbone. Hence, we must depart from this "particle-in-a-box model" view, and notice that it is the magnitude of the electron–hole displacement, $R_{e\text{-}h}$, that distinguishes the two systems: The mean $\langle R_{e\text{-}h} \rangle$ is reduced in PDOPT (0.11 repeating units) with respect to P3HT (0.45 repeating units); see Fig. 3*E*. We recall that the transition energy of conjugated polymers does not depend only on the coherence length but also on the electronic π-overlap coupling (or conjugation) between repeating units. Given that the mean coherence lengths are similar in both materials, the reduced transition energy in single PDOPT necessarily implies a stronger electronic coupling in this system, which is witnessed by the smaller calculated $R_{e\text{-}h}$ (29). Computationally, for the more disordered P3HT, the wave function of the lowest excited state is dominated by Slater determinants describing the promotion of an electron from HOMO to LUMO as well as from HOMO to LUMO+1. In particular, the latter results in a more pronounced charge transfer character of the excited state in

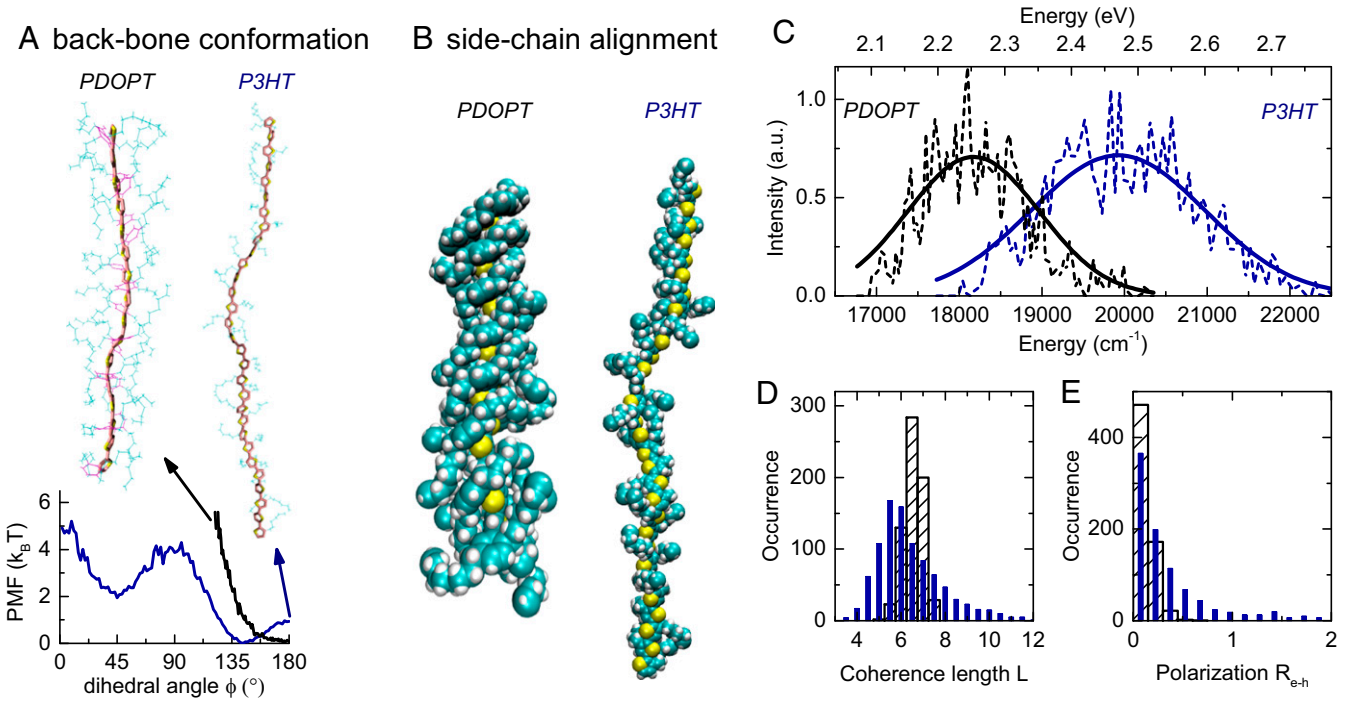

Fig. 3. Quantum-classical atomistic simulations of the conformational, optical, and electronic properties of single PDOPT and P3HT chains. (*A*) (*Top*) Snapshots from trajectories of PDOPT16 and P3HT30 chains highlighting the backbone conformation. (*Bottom*) Corresponding PMF as a function of the dihedral angle ϕ (blue, P3HT; black, PDOPT). (*B*) Snapshots showing the side-chain alignment of the two polythiophenes. (*C*) Dashed lines denote calculated absorption spectra from thermal ensembles of PDOPT (black) and P3HT (blue). Solid lines denote Gaussian fits to the calculated spectra. (*D* and *E*) Distribution of (*D*) coherence lengths L and (*E*) electron–hole separation distances $R_{e\text{-}h}$ (both in number of repeating units) for P3HT (solid blue) and PDOPT (hatched black).

P3HT. For PDOPT, in contrast, the relative contribution of Slater determinants for the HOMO to LUMO+1 promotion is significantly reduced. Hence, the higher degree of planarity in PDOPT enhances conjugation, which results in more tightly bound excitons with less pronounced charge transfer character (reduced $R_{e\text{-}h}$), compared with P3HT. For further details, see the discussion of the polarization index parameter D in our recent work (29).

In this context, we note that, according to the simplified models of Spano, Barford, and coworkers (57, 58), the ratio between the area of the ZPL and the area of the effective vibrational mode (here around 1,480 cm^{-1}) in the experimental spectra is usually interpreted as a measure for the coherence length L of the absorbing/emitting sites, with a relatively stronger ZPL indicating a larger L. From such analysis, we find an increase in coherence length by roughly a factor of 2 from the disordered P3HT to the more planar PDOPT (Fig. S4), in agreement with common notion, but in contrast to our results of a direct calculation. Although largely ignored in the literature, the framework developed by Spano and coworkers (57, 59) also allows for the possibility to account for different peak ratios by distinct electron–hole separations for a given coherence length. Consistent with our results, a larger electron–hole distance is predicted to give rise to a decreased peak ratio between the ZPL and the vibrational mode (*SI Coherence Length of the Emitting Site*). We conclude that the experimental ratio between ZPL and the effective vibrational mode may rather reflect the strength of the conjugation controlled by backbone conformation, but not the coherence length. Finally, we emphasize that this shifts the discussion from the comparison of coherence lengths in two materials to a discussion of a so far overlooked physical quantity affected by the conjugation, the electron–hole polarization.

Conclusion

Based on our combined experimental and theoretical investigation of the two polythiophene derivatives PDOPT and P3HT on the single-chain and bulk level, we have demonstrated that, contrary to common notion, the bulky side groups of PDOPT actually induce a stable planarization of the conjugated backbone via noncovalent interactions. This more planar backbone leads to a red shift of >2,000 cm^{-1} (0.25 eV) of its electronic transition relative to that in the more conformationally disordered P3HT single chains. Intriguingly, this side-chain induced planarization does not give rise to an increase in mean coherence length (spatial extent of the absorbing/emitting sites), which is essentially identical for both polythiophenes. It is rather the conjugation, i.e., the electronic π-overlap between thiophene rings, that is stronger in PDOPT, and ultimately causes the observed red shift in transition energy and reduces the electron–hole polarization.

Our spectroscopic data strongly indicate that the bulky dioctylphenyl side groups of PDOPT have a strong impact on the static and dynamic disorder, and must be involved in planarization. According to our simulations of single chains, their phenyl rings are rotated ∼90° out of the backbone plane (Fig. 3*A*). Recent work on arene–thiophene systems suggests that such a T-shaped arrangement is indeed a stable, energetically favorable configuration (60). In PDOPT, this orientation is arguably further stabilized by the interaction between the *n*-octyl side chains which extend across its backbone. The importance of the side groups for structural properties in PDOPT is also manifest in its crystallization behavior. Despite the absence of π–π stacking, spherulitic structures of several hundred micrometers diameter and a high degree of crystallinity can be grown under appropriate conditions (61). The main driving forces for spherulite formation are noncovalent interactions between side groups of neighboring chains (20). In the resulting configuration, the phenyl rings and *n*-octyl chains are oriented perpendicularly to the plane of the backbones, with a dense interdigitation of adjacent *n*-octyl chains (62). Interestingly, the concept of side-chain induced stabilization of polymers' secondary and tertiary structures is also known in biological systems. Interactions of side groups, such as aromatic–aromatic interactions, routinely lead to a stabilization of the ternary structure of proteins (63, 64). Such interactions are also conceivable between adjacent phenyl rings of a PDOPT chain, with a mean distance slightly larger than ∼7 Å in spherulites (20).

Further studies are clearly required to develop broader insight into the structural variation obtainable via side-chain manipulation. The backbone planarization in PDOPT suggests that this control may ultimately pave the road for the design of optimized structures for efficient optoelectronics applications.

Methods and Materials

Experimental Methods. Single-molecule PL experiments on PDOPT were performed employing a home-built confocal microscope, as reported recently (22). For sample preparation, PDOPT was diluted in *n*-hexadecane, shock-frozen in liquid nitrogen, and subsequently cooled down to 1.5 K in a home-built bath cryostat. For each chain, we measured up to 500 sequential spectra with an integration time of 1 s to 3 s each. Temperature-dependent ensemble PL spectra were measured in a home-built setup described in detail elsewhere (65). In brief, the polymers were dissolved in THF, and the sample was placed in an electrically heatable continuous flow cryostat. Each temperature was stabilized for 15 min before measurement to ensure a homogeneous temperature across the sample. See *SI Methods and Materials* for details.

Materials. To synthesize PDOPT with a defined molecular weight, low dispersity, and high regioregularity, a Kumada catalyst-transfer polycondensation including a nickel catalyst with a hybrid P,N ligand was used (21). P3HT was synthesized via catalyst transfer polymerization (66). Both PDOPT and P3HT contain only a single regiodefect at one end of each chain which is introduced by the synthetic route (23, 66, 67).

Simulation. To compare the optical properties of single-molecule P3HT with those of PDOPT, we repeated the calculation recently published by two of us in ref. 29. The polymers were modeled with a nonpolar environment through the alkane-like dielectric constant $\varepsilon = 2.7$. The relevant properties of the lowest energy excited state, i.e., the coherence length L and the electron–hole displacement distance $R_{e\text{-}h}$, were derived using the CIS mixed density matrix. Importantly, since the side chains in both thiophenes are not expected to contribute to the spectrum in the relevant energy window, they were modeled via classical equations of motion with an appropriate force field. In P3HT, this is justified due to the alkyl character of the side chains, while, in PDOPT, the conjugation between the thiophene backbone and the substituted aromatic phenyl rings is broken due to steric interactions in our simulations at all times. See *SI Simulation Protocol* for details.

ACKNOWLEDGMENTS. We thank Marin van Heel (University of Leiden, Leiden, Netherlands) for providing the multivariate statistical analysis algorithm for data analysis. D.R. thanks Thiago B. de Queiroz for helpful discussions. This work was financially supported by the German Research Foundation through Projects HI1508/2 (to D.R., S.B., and R.H.), SO1213/5-1 (to D.S. and M.S.), and GRK1640 (to D.R., F.P., S.B., J.K., A.K., M.T., and R.H.). Additional funding came from the Bavarian State Ministry of Science, Research and the Arts for the collaborative research network Solar Technologies Go Hybrid (J.K., M.T., and A.K.). R.H. acknowledges support from the Elite Network of Bavaria "Macromolecular Science." P.J.R. is grateful for the support of the National Science Foundation (CHE-1362381).

1. Huang Y, Kramer EJ, Heeger AJ, Bazan GC (2014) Bulk heterojunction solar cells: Morphology and performance relationships. *Chem Rev* 114:7006–7043.
2. Noriega R, et al. (2013) A general relationship between disorder, aggregation and charge transport in conjugated polymers. *Nat Mater* 12:1038–1044.
3. Hildner R, Köhler A, Müller-Buschbaum P, Panzer F, Thelakkat M (2017) π-conjugated donor polymers. Structure formation and morphology in solution, bulk and photovoltaic blends. *Adv Energy Mater* 7:1700314.
4. Hu Z, et al. (2017) Impact of backbone fluorination on nanoscale morphology and excitonic coupling in polythiophenes. *Proc Natl Acad Sci USA* 114:5113–5118.
5. Milián-Medina B, Gierschner J (2017) "Though it be but little, it is fierce": Excited state engineering of conjugated organic materials by fluorination. *J Phys Chem Lett* 8:91–101.
6. Mei J, Bao Z (2014) Side chain engineering in solution-processable conjugated polymers. *Chem Mater* 26:604–615.

7. Mueller CJ, Gann E, Singh CR, Thelakkat M, McNeill CR (2016) Control of molecular orientation in polydiketopyrrolopyrrole copolymers via diffusive noncovalent interactions. *Chem Mater* 28:7088–7097.
8. Himmelberger S, et al. (2015) Role of side-chain branching on thin-film structure and electronic properties of polythiophenes. *Adv Funct Mater* 25:2616–2624.
9. Jackson NE, et al. (2013) Controlling conformations of conjugated polymers and small molecules: The role of nonbonding interactions. *J Am Chem Soc* 135:10475–10483.
10. Mueller CJ, Singh CR, Fried M, Huettner S, Thelakkat M (2015) High bulk electron mobility diketopyrrolopyrrole copolymers with perfluorothiophene. *Adv Funct Mater* 25:2725–2736.
11. Lombeck F, et al. (2016) PCDTBT: From polymer photovoltaics to light-emitting diodes by side-chain-controlled luminescence. *Macromolecules* 49:9382–9387.
12. Schlüter AD, Rabe JP (2000) Dendronized polymers: Synthesis, characterization, assembly at interfaces, and manipulation. *Angew Chem Int Ed Engl* 39:864–883.
13. Vezie MS, et al. (2016) Exploring the origin of high optical absorption in conjugated polymers. *Nat Mater* 15:746–753.
14. Strickler SJ, Berg RA (1962) Relationship between absorption intensity and fluorescence lifetime of molecules. *J Chem Phys* 37:814–822.
15. Milad R, et al. (2016) Effective conjugation in conjugated polymers with strongly twisted backbones. A case study on fluorinated MEHPPV. *J Mater Chem C* 4: 6900–6906.
16. Panzer F, Bässler H, Köhler A (2017) Temperature induced order-disorder transition in solutions of conjugated polymers probed by optical spectroscopy. *J Phys Chem Lett* 8: 114–125.
17. Andersson MR, et al. (1999) Substituted polythiophenes designed for optoelectronic devices and conductors. *J Mater Chem* 9:1933–1940.
18. Ko S, et al. (2012) Controlled conjugated backbone twisting for an increased open-circuit voltage while having a high short-circuit current in poly(hexylthiophene) derivatives. *J Am Chem Soc* 134:5222–5232.
19. Kuei B, Gomez ED (2016) Chain conformations and phase behavior of conjugated polymers. *Soft Matter* 13:49–67.
20. Hamidi-Sakr A, et al. (2016) Highly oriented and crystalline films of a phenyl-substituted polythiophene prepared by epitaxy. Structural model and influence of molecular weight. *Macromolecules* 49:3452–3462.
21. Schiefer D, et al. (2014) Nickel catalyst with a hybrid P, N ligand for Kumada catalyst transfer polycondensation of sterically hindered thiophenes. *ACS Macro Lett* 3: 617–621.
22. Raithel D, et al. (2016) Emitting species of poly(3-hexylthiophene): From single, isolated chains to bulk. *Macromolecules* 49:9553–9560.
23. Kohn P, et al. (2012) On the role of single regiodefects and polydispersity in regioregular poly(3-hexylthiophene): Defect distribution, synthesis of defect-free chains, and a simple model for the determination of crystallinity. *J Am Chem Soc* 134: 4790–4805.
24. Brinkmann M (2011) Structure and morphology control in thin films of regioregular poly(3-hexylthiophene). *J Polym Sci B Polym Phys* 49:1218–1233.
25. Clark J, Silva C, Friend RH, Spano FC (2007) Role of intermolecular coupling in the photophysics of disordered organic semiconductors: Aggregate emission in regioregular polythiophene. *Phys Rev Lett* 98:206406.
26. Thiessen A, et al. (2013) Unraveling the chromophoric disorder of poly(3-hexylthiophene). *Proc Natl Acad Sci USA* 110:E3550–E3556.
27. Hu Z, et al. (2013) Effect of the side-chain-distribution density on the single-conjugated-polymer-chain conformation. *ChemPhysChem* 14:4143–4148.
28. Chen P-Y, Rassamesard A, Chen H-L, Chen S-A (2013) Conformation and fluorescence property of poly(3-hexylthiophene) isolated chains studied by single molecule spectroscopy: Effects of solvent quality and regioregularity. *Macromolecules* 46: 5657–5663.
29. Simine L, Rossky PJ (2017) Relating chromophoric and structural disorder in conjugated polymers. *J Phys Chem Lett* 8:1752–1756.
30. Hildner R, Lemmer U, Scherf U, van Heel M, Köhler J (2007) Revealing the electron–phonon coupling in a conjugated polymer by single-molecule spectroscopy. *Adv Mater* 19:1978–1982.
31. Hildner R, Winterling L, Lemmer U, Scherf U, Köhler J (2009) Single-molecule spectroscopy on a ladder-type conjugated polymer: Electron-phonon coupling and spectral diffusion. *ChemPhysChem* 10:2524–2534.
32. Brambilla L, et al. (2014) Regio-regular oligo and poly(3-hexyl thiophene): Precise structural markers from the vibrational spectra of oligomer single crystals. *Macromolecules* 47:6730–6739.
33. Becker RS, Seixas de Melo J, Maçanita AL, Elisei F (1996) Comprehensive evaluation of the absorption, photophysical, energy transfer, structural, and theoretical properties of α-oligothiophenes with one to seven rings. *J Phys Chem* 100:18683–18695.
34. Gierschner J, Cornil J, Egelhaaf H-J (2007) Optical bandgaps of π-conjugated organic materials at the polymer limit: Experiment and theory. *Adv Mater* 19:173–191.
35. Rossi G, Chance RR, Silbey R (1989) Conformational disorder in conjugated polymers. *J Chem Phys* 90:7594–7601.
36. de Queiroz TB, Kümmel S (2015) Tuned range separated hybrid functionals for solvated low bandgap oligomers. *J Chem Phys* 143:034101.
37. Baderschneider S, Scherf U, Köhler J, Hildner R (2016) Influence of the conjugation length on the optical spectra of single ladder-type (p-phenylene) dimers and polymers. *J Phys Chem A* 120:233–240.
38. Ambrose WP, Moerner WE (1991) Fluorescence spectroscopy and spectral diffusion of single impurity molecules in a crystal. *Nature* 349:225–227.
39. Feist FA, Basché T (2008) Fluorescence excitation and emission spectroscopy on single MEH-PPV chains at low temperature. *J Phys Chem B* 112:9700–9708.
40. Pullerits T, Mirzov O, Scheblykin IG (2005) Conformational fluctuations and large fluorescence spectral diffusion in conjugated polymer single chains at low temperatures. *J Phys Chem B* 109:19099–19107.
41. Westenhoff S, et al. (2006) Anomalous energy transfer dynamics due to torsional relaxation in a conjugated polymer. *Phys Rev Lett* 97:166804.
42. Kador L (1991) Stochastic theory of inhomogeneous spectroscopic line shapes reinvestigated. *J Chem Phys* 95:5574–5581.
43. Hoffmann ST, Bässler H, Köhler A (2010) What determines inhomogeneous broadening of electronic transitions in conjugated polymers? *J Phys Chem B* 114: 17037–17048.
44. Marcus M, Tozer OR, Barford W (2014) Theory of optical transitions in conjugated polymers. II. Real systems. *J Chem Phys* 141:164102.
45. Kobayashi H, Tsuchiya K, Ogino K, Vacha M (2012) Spectral multitude and spectral dynamics reflect changing conjugation length in single molecules of oligophenylenevinylenes. *Phys Chem Chem Phys* 14:10114–10118.
46. Geva E, Skinner JL (1997) Theory of single-molecule optical line-shape distributions in low-temperature glasses. *J Phys Chem B* 101:8920–8932.
47. Kador L, Horne DE, Moerner WE (1990) Optical detection and probing of single dopant molecules of pentacene in a p-terphenyl host crystal by means of absorption spectroscopy. *J Phys Chem* 94:1237–1248.
48. Orrit M, Bernard J (1990) Single pentacene molecules detected by fluorescence excitation in a p-terphenyl crystal. *Phys Rev Lett* 65:2716–2719.
49. Bhatta RS, Tsige M, Perry DS (2014) Torsionally-induced blue shift of the band gap in poly(3-hexylthiophene). *J Comput Theor Nanosci* 11:2157–2164.
50. Renger T, Grundkötter B, Madjet M-A, Müh F (2008) Theory of solvatochromic shifts in nonpolar solvents reveals a new spectroscopic rule. *Proc Natl Acad Sci USA* 105: 13235–13240.
51. Renge I (1992) Relationship between electron–phonon coupling and intermolecular interaction parameters in dye-doped organic glasses. *J Opt Soc Am B* 9:719–723.
52. Athanasopoulos S, Hoffmann ST, Bässler H, Köhler A, Beljonne D (2013) To hop or not to hop? Understanding the temperature dependence of spectral diffusion in organic semiconductors. *J Phys Chem Lett* 4:1694–1700.
53. Warshel A, Karplus M (1972) Calculation of ground and excited state potential surfaces of conjugated molecules. I. Formulation and parametrization. *J Am Chem Soc* 94:5612–5625.
54. Lobaugh J, Rossky PJ (1999) Computer simulation of the excited state dynamics of betaine-30 in acetonitrile. *J Phys Chem A* 103:9432–9447.
55. Darling SB, Sternberg M (2009) Importance of side chains and backbone length in defect modeling of poly(3-alkylthiophenes). *J Phys Chem B* 113:6215–6218.
56. Barford W, Lidzey DG, Makhov DV, Meijer AJ (2010) Exciton localization in disordered poly(3-hexylthiophene). *J Chem Phys* 133:044504, and correction (2010) 133:119901.
57. Spano FC, Silva C (2014) H- and J-aggregate behavior in polymeric semiconductors. *Annu Rev Phys Chem* 65:477–500.
58. Barford W, Marcus M (2017) Perspective: Optical spectroscopy in π-conjugated polymers and how it can be used to determine multiscale polymer structures. *J Chem Phys* 146:130902.
59. Hestand NJ, Spano FC (2016) Determining the spatial coherence of excitons from the photoluminescence spectrum in charge-transfer J-aggregates. *Chem Phys* 481: 262–271.
60. Castellano O, Gimon R, Soscun H (2011) Theoretical study of the σ–π and π–π interactions in heteroaromatic monocyclic molecular complexes of benzene, pyridine, and thiophene dimers. Implications on the resin–asphaltene stability in crude oil. *Energy Fuels* 25:2526–2541.
61. Keheze FM, et al. (2017) Signatures of melting and recrystallization of a bulky substituted poly(thiophene) identified by optical spectroscopy. *Macromolecules* 50: 6829–6839.
62. Aasmundtveit KE, et al. (2000) Structural ordering in phenyl-substituted polythiophenes. *Macromolecules* 33:5481–5489.
63. Burley SK, Petsko GA (1985) Aromatic-aromatic interaction: A mechanism of protein structure stabilization. *Science* 229:23–28.
64. Salonen LM, Ellermann M, Diederich F (2011) Aromatic rings in chemical and biological recognition: Energetics and structures. *Angew Chem Int Ed Engl* 50: 4808–4842.
65. Panzer F, et al. (2016) Reversible laser-induced amplified spontaneous emission from coexisting tetragonal and orthorhombic phases in hybrid lead halide perovskites. *Adv Opt Mater* 4:917–928.
66. Lohwasser RH, Thelakkat M (2011) Toward perfect control of end groups and polydispersity in poly(3-hexylthiophene) via catalyst transfer polymerization. *Macromolecules* 44:3388–3397.
67. Schiefer D, et al. (2016) Poly(3-(2,5-dioctylphenyl)thiophene) synthesized by direct arylation polycondensation. End groups, defects, and crystallinity. *Macromolecules* 49:7230–7237.